

RESEARCH ARTICLE

10.1002/2016GC006407

Key Points:

- The relative downward offset of loess pDRM is semiquantitatively estimated
- A refined pDRM acquisition model for the Matuyama-Brunhes reversal in Chinese loess is proposed
- Paleoprecipitation is suggested to be the dominant factor controlling the loess pDRM acquisition processes

Supporting Information:

- Supporting Information S1

Correspondence to:

Q. S. Liu,
qslu@mail.iggcas.ac.cn

Citation:

Jin, C., Q. Liu, P. Hu, Z. Jiang, C. Li, P. Han, H. Yang, and W. Liang (2016), An integrated natural remanent magnetization acquisition model for the Matuyama-Brunhes reversal recorded by the Chinese loess, *Geochem. Geophys. Geosyst.*, *17*, 3150–3163, doi:10.1002/2016GC006407.

Received 21 APR 2016

Accepted 14 JUN 2016

Accepted article online 12 JUL 2016

Published online 10 AUG 2016

An integrated natural remanent magnetization acquisition model for the Matuyama-Brunhes reversal recorded by the Chinese loess

Chunsheng Jin^{1,2}, Qingsong Liu^{1,3}, Pengxiang Hu¹, Zhaoxia Jiang¹, Cange Li¹, Peng Han¹, Huihui Yang¹, and Wentian Liang⁴

¹Institute of Geology and Geophysics, Chinese Academy of Sciences, Beijing, China, ²CAS Center for Excellence in Tibetan Plateau Earth Sciences, Beijing, China, ³Laboratory for Marine Geology, Qingdao National Oceanography Laboratory for Science and Technology, Qingdao, China, ⁴State Key Laboratory of Continental Dynamics, Northwest University, Xi'an, China

Abstract Geomagnetic polarity reversal boundaries are key isochronous chronological controls for the long Chinese loess sequences, and further facilitate paleoclimatic correlation between Chinese loess and marine sediments. However, owing to complexity of postdepositional remanent magnetization (pDRM) acquisition processes related to variable dust sedimentary environments on the Chinese Loess Plateau (CLP), there is a long-standing dispute concerning the downward shift of the pDRM recorded in Chinese loess. In this study, after careful stratigraphic correlation of representative climatic tie points and the Matuyama-Brunhes boundaries (MBB) in the Xifeng, Luochuan, and Mangshan loess sections with different pedogenic environments, the downward shift of the pDRM is semiquantitatively estimated and the acquisition model for the loess natural remanent magnetization (NRM) is discussed. The measured MB transition zone has been affected by the surficial mixing layer (SML) and remagnetization. Paleoprecipitation is suggested to be the dominant factor controlling the pDRM acquisition processes. Rainfall-controlled leaching would restrict the efficiency of the characterized remanent magnetization carriers aligning along the ancient geomagnetic field. We conclude that the MBB in the central CLP with moderate paleoprecipitation could be considered as an isochronous chronological control after moderate upward adjustment. A convincing case can then be made to correlate L8/S8 to MIS 18/19.

1. Introduction

The Quaternary Chinese loess-paleosol sequences, as one of the most continuous terrestrial sediments, which can be traced backward at least to the past 2.8 Ma [Yang and Ding, 2010], preserve high-resolution records of paleoclimate variability, and detailed geomagnetic field behaviors on different time scales [e.g., Porter and An, 1995; Ding et al., 2002; Sun et al., 2011; Liu et al., 2015]. The first-order chronological framework of Chinese loess was constructed based mainly on magnetostratigraphy [Heller and Liu, 1982]. Geomagnetic polarity reversal boundaries have been usually used as key isochronous chronological controls while orbital tuning an astronomical loess timescale [e.g., Ding et al., 1994; Lu et al., 1999; Heslop et al., 2000; Sun et al., 2006]. Determining an accurate stratigraphic location of reversal boundaries in loess is essential for precise orbital tuning. However, owing to complex postdepositional remanent magnetization (pDRM) acquisition processes and variable dust sedimentary environments, pDRM in Chinese loess may be fixed with a time lag, resulting in an unknown pDRM lock-in depth [Spassov et al., 2003; Liu et al., 2008; Sun et al., 2013; Wang et al., 2014; Zhao et al., 2014; Zhou et al., 2014].

There is a long-standing dispute concerning the pDRM lock-in depth, such as a large-scale ranging from few tens to 300 cm [e.g., Tauxe et al., 1996; Zhou and Shackleton, 1999; Heslop et al., 2000; Spassov et al., 2003; Zhou et al., 2014], or a small and negligible lock-in depth [e.g., Zhu et al., 1994a, 1998, 2006; Pan et al., 2002; Wang et al., 2006; Yang et al., 2007b, 2008, 2010; Liu et al., 2008]. Besides the lock-in processes of pDRM, surficial mixing layer (SML) would also move polarity boundaries downward. For examples, rainfall-controlled leaching in Sanmenxia area [Wang et al., 2005] resulted in rotation of characteristic remanent magnetization (ChRM) carriers and further caused remagnetization in L9. Meanwhile, magnetic particles carried ChRM

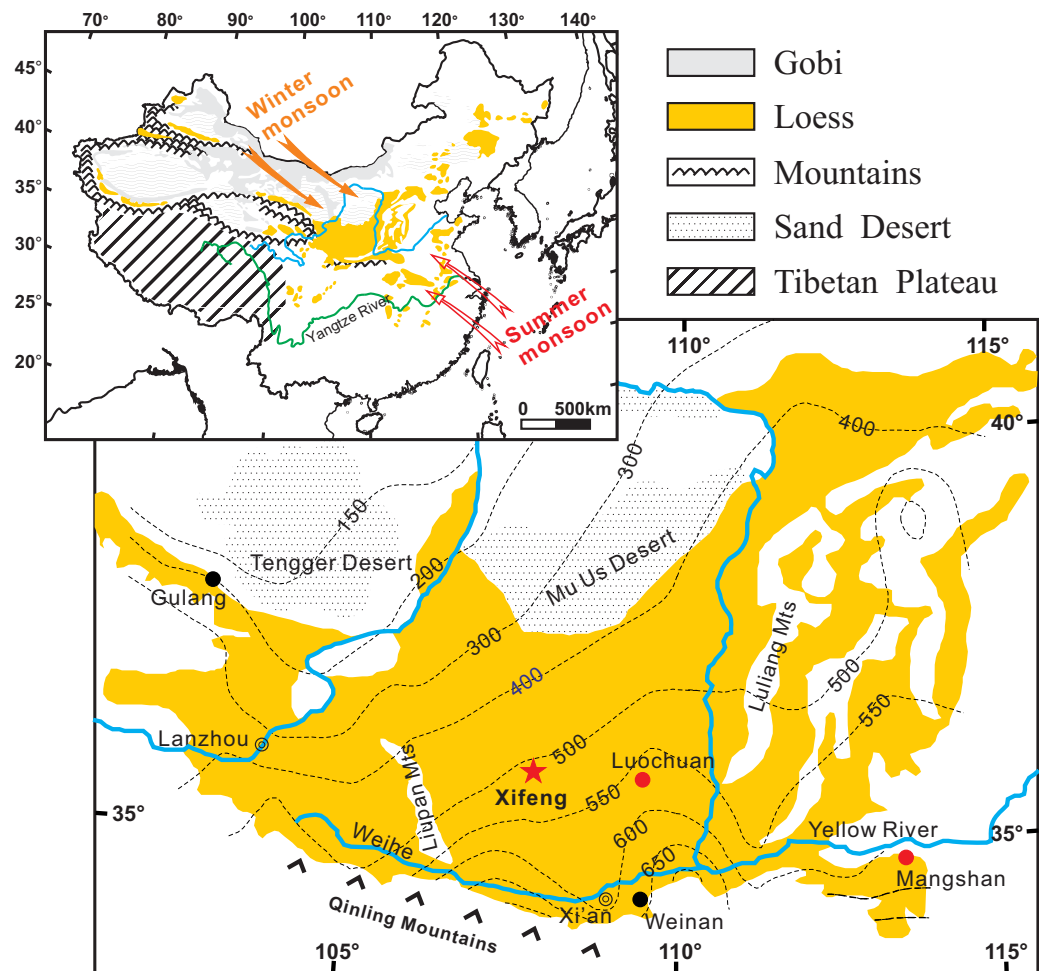


Figure 1. A schematic map of the distribution of the Chinese loess and the location of the Xifeng (XF) (star), Luochuan (LC), Mangshan (MS) sections (red dots). Black dots represent the other sections mentioned in the text. Black dashed lines represent MAP in the studied area.

should be first shifted downward through the SML and then can be fixed during subsequent lock-in processes [Liu *et al.*, 2008]. Therefore, downward offset of the pDRM may be a complicated result related to many factors.

To quantify the downward offset of the pDRM, it is necessary to determine the true position of the reversal boundaries in Chinese loess. Using optically stimulated luminescence ages, the spatial downward offset of the Laschamp excursion recorded by the Chinese loess has been discussed [Sun *et al.*, 2013]. Nevertheless, it is still difficult to directly evaluate such effects due to a lack of absolute dating for older loess deposits. For the Quaternary geomagnetic reversal records in loess, the Matuyama-Brunhes Boundary (MBB) has been well investigated [e.g., Zhu *et al.*, 1994a; Spassov *et al.*, 2001; Jin and Liu, 2010; Yang *et al.*, 2010; Wang *et al.*, 2014]. In this study, we systematically investigate the MBBs recorded in the Xifeng (XF), Luochuan (LC), and Mangshan (MS) loess sections spatially distributed in different climatic regions in the CLP. We aim to semiquantitatively estimate the relative pDRM downward offset depth for the MBB and to further discuss factors potentially influencing the offset effect. Finally, a refined pDRM acquisition model is proposed.

2. Sampling and Measurements

Samples from S7 to L9 at Xifeng (35°45′37.8″N, 107°46′20.43″E) (Figure 1) with a total thickness of 620 cm (Figure 2a) are collected after removing the surface weathered material. Oriented blocks are sampled in the interval of 30–420 cm and are oriented in situ using a magnetic compass with a north direction marked on the top surface. Five sets of parallel samples covering the MBB are obtained followed the procedure of

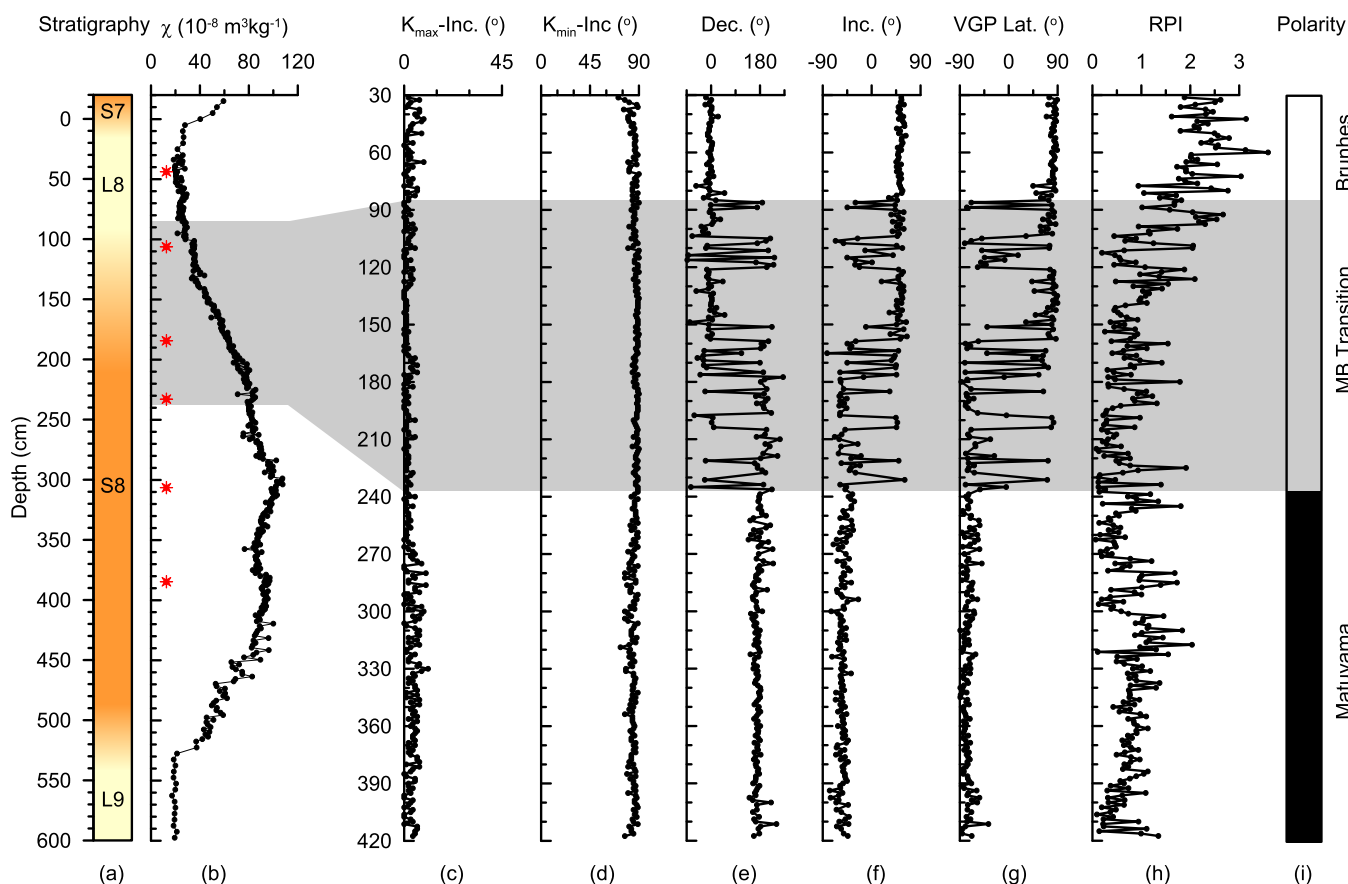


Figure 2. (a) Stratigraphy for XF sampled interval; (b) mass-specific low-field susceptibility (χ); (c) inclination of maximum-susceptibility axis (K_{\max} -Inc.); (d) inclination of minimum-susceptibility axis (K_{\min} -Inc.); (e) declination (Dec.) of characteristic remanent magnetization (ChRM); (f) inclination (Inc.) of ChRM; (g) virtual geomagnetic pole latitude (VGP-Lat.); (h) relative paleointensity (RPI); (i) magnetic polarity. The Matuyama-Brunhes (MB) transitional interval of paleomagnetic directions is shaded in gray. Red stars represent bulk samples selected for detailed rock magnetic analysis.

Jin and Liu [2010]. The present mean annual precipitation (MAP) in XF and LC areas is about 400–600 mm. The MAP is larger in LC than in XF. The MAP in MS area is about 640 mm.

The mass-specific low-field magnetic susceptibility (χ) of 386 bulk samples is measured using a Bartington MS2 Susceptibility Meter. One set of oriented samples is first thermally demagnetized to locate the probable MBB. Then the other four parallel sample sets (A–D) between 60 and 260 cm are demagnetized to define the exact position of the MB transitional zone. Totally, 712 oriented specimens are progressively thermal demagnetized from room temperature up to 585 or 680°C in steps of 10–50°C using a Magnetic Measurements Thermal Demagnetizer (MMTD80) with a residual magnetic field of <10 nT. All remanence are measured using a 2G Enterprises model 760 cryogenic magnetometer installed in a magnetically shielded room (<300 nT) in IGGCAS. The anisotropy of magnetic susceptibility (AMS) for all the oriented samples is measured using a KLY-3s Kappa bridge (AGICO Ltd.) before thermal treatment. Six representative bulk samples are selected for detailed rock magnetic analysis (red stars in Figure 2b). Temperature-dependent susceptibility (χ -T) curves are measured using an MFK1-FA Kappa bridge (AGICO Ltd.) equipped with a CS-4 high-temperature furnace going from room temperature up to 700°C in an argon atmosphere (the flow rate is about 100 mL/min) to prevent possible oxidation upon heating. Temperature-dependent saturation magnetization (M_s -T) curves are measured using a Variable Field Translation Balance (VFTB) system (Petersen Instruments). Samples for M_s -T curves are heated in air using a field of 1 T. The temperature sweeping rate is 40°C/min. Isothermal remanent magnetization (IRM) acquisition curves (with a maximum field of 1.5 T), backfield demagnetization curves, and hysteresis parameters [including the M_s , saturation remanence (M_{rs}), coercivity (B_c), and coercivity of remanence (B_{cr})] are measured using a Princeton Measurements Vibrating Sample Magnetometer (VSM3900, Princeton Measurements Corp.). Hysteretic parameters are obtained after subtraction of the paramagnetic contribution.

3. Results

3.1. Rock Magnetism Results

The χ -T curve has been widely used as a routine rock magnetic tool to identify magnetic mineralogy and possible mineral transformation upon heating. The χ -T curves for representative samples (Figures 3a–3f) exhibit a major decrease in susceptibility at about 585°C which indicates the presence of magnetite. At lower temperatures (<300°C) the susceptibility curves increase slowly owing to the unblocking of single domain phases and decrease steadily between 300 and 400°C due to transformation of maghemite to weakly magnetic hematite [e.g., Deng *et al.*, 2000, 2005, 2006; Liu *et al.*, 2005]. The χ after cooling is always several times higher than the initial values before heating, which is generally attributed to the neoformation of magnetite grains from iron-containing silicates/clays, or due to the formation of magnetite by reduction as a result of the burning of organic matter [Hunt *et al.*, 1995; Deng *et al.*, 2000, 2005, 2006; Liu *et al.*, 2005].

The M_s -T curve is generally preferred for determining the Curie temperature of natural samples. It is irreversible for M_s -T curves during heating and cooling, with identifiable signals of paramagnetic contributions at high temperature (Figures 3g–3i). The inflexions in the M_s -T curves at about 580°C further suggest the Curie point of magnetite. The slight “concavity” between about 300 and 500°C is generally identified as the existence of metastable maghemite, which could transform easily to hematite in this temperature interval [Liu *et al.*, 2003; Wang *et al.*, 2005; Yang *et al.*, 2008, 2010]. Stepwise acquisition of IRM curve is identical for all samples (Figure 4a). They climb rapidly below 200 mT and reach saturation at about 300 mT. This behavior reveals the existence of soft magnetic minerals, such as magnetite and/or maghemite. Slight increase of IRM from 300 mT up to 1.5 T indicates the presence of hard magnetic components, such as hematite and/or goethite.

After subtracting the paramagnetic contribution, all the hysteresis loops display a weakly wasp-waisted shape, representing a mixture of magnetic minerals with low and high coercivity (Figure 4c) [Roberts *et al.*, 1995]. Hysteresis parameter ratios (M_r/M_s , B_{cr}/B_c) were plotted on a Day plot [Day *et al.*, 1977; Dunlop, 2002] to determine the domain state of magnetic minerals in samples (Figure 4d). All plots are constrained in a pseudo-single domain (PSD) area and cluster closely. This indicates that the mean grain size of magnetic minerals in samples is rather uniform across the sampled interval.

3.2. Paleomagnetic Results

Demagnetization data are treated with principal component analysis using the PaleoMag software (version 3.1d40) developed by Craig H. Jones and Joya Tetreault. Orthogonal projections of representative samples are shown in Figure 5. Two components can be clearly defined for samples with the reversed polarity. The low-temperature component is a viscous remanent magnetization (VRM) and can be thermally demagnetized at 200–300°C [Heller and Liu, 1982; Pan *et al.*, 2001; Wang *et al.*, 2005]. The ChRM for most of the samples (93.8%) was isolated above 300°C calculated by a least squares fitting technique [Kirschvink, 1980]. The maximum angular deviation is <15°.

The AMS results, especially the inclination of the maximum (K_{\max} -Inc) and minimum (K_{\min} -Inc) axes of the susceptibility ellipsoid, have been widely used to detect postdepositional disturbance [e.g., Zhu *et al.*, 1999, 2004; Wang *et al.*, 2005; Yang *et al.*, 2008, 2010]. In this study, the K_{\max} -Inc values are <11° (Figure 2c), and 99% of the K_{\min} -Inc are >75°, approximately perpendicular to the horizontal plane (Figure 2d). The shape of the AMS ellipsoid is oblate and is controlled mainly by foliation ($F > 1.004$). This indicates that magnetic fabrics of the studied sediments represent a primary sedimentary fabric without apparent disorders and disturbances.

Using five sets of parallel samples, the MB transitional zone is compositively determined in the interval of 81.25–243.75 cm with a thickness of 162.5 cm (Figure 6), which is located in the stratigraphic transition zone of L8 and S8. This pattern is consistent with results from LC [Jin and Liu, 2010] and MS [Jin and Liu, 2011a]. The relative intensity (RPI) is estimated by NRM_{300}/χ as Yang *et al.* [2010], where NRM_{300} is the residual NRM after 300°C thermal demagnetization. Clearly, the MB transitional zone corresponds to the low RPI values (Figure 2h).

3.3. Estimation of Downward pDRM Offset

The low-field susceptibility of Chinese loess has been considered as an excellent proxy of the East Asian summer monsoon, with higher values in paleosol units due to the neoformation of ultra fine-grained

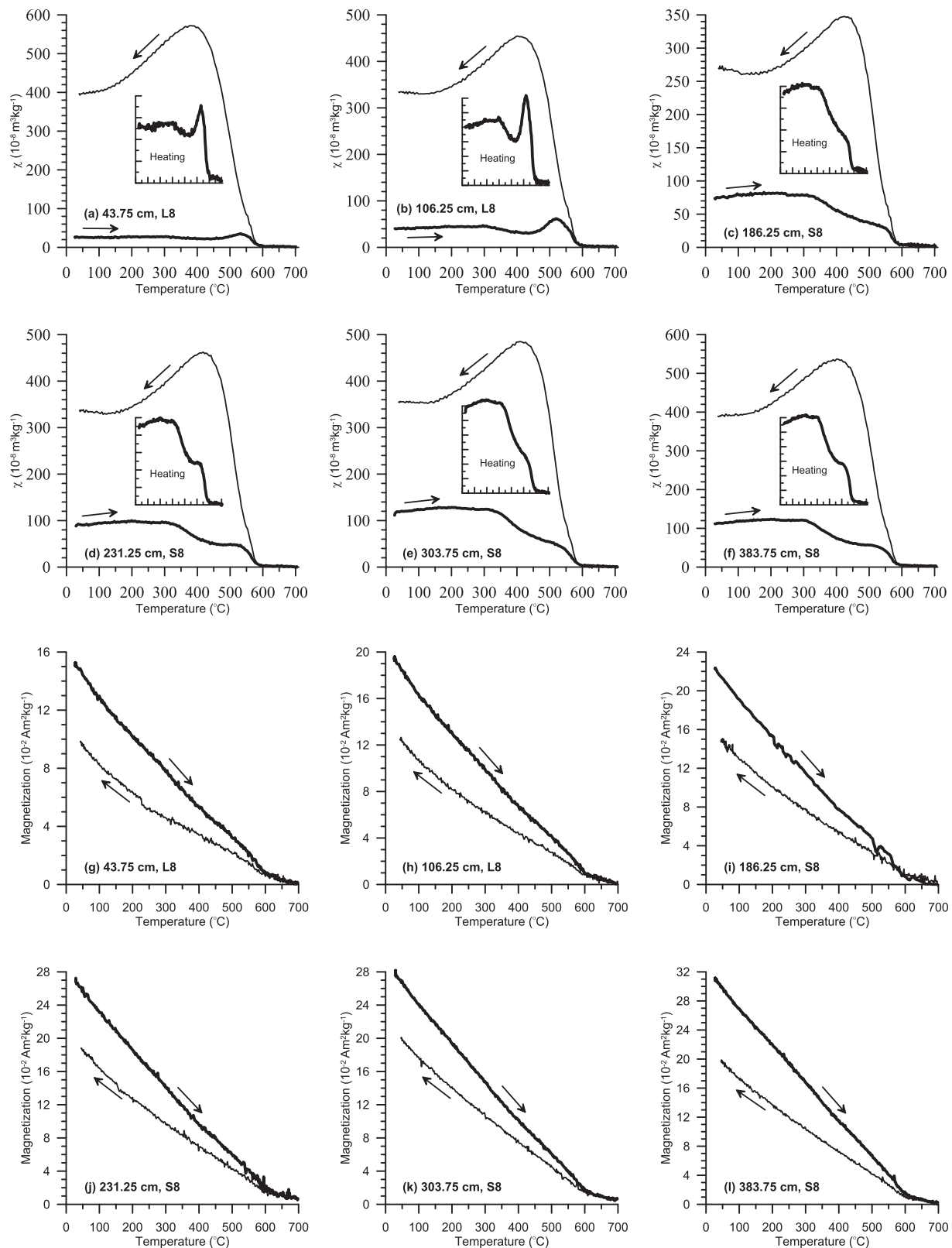


Figure 3. (a–f) Temperature dependence of magnetic susceptibility and (g–l) high-temperature magnetization for representative samples. Samples at 43.75 and 106.25 cm are from L8, and others from S8. Thicker lines indicate heating runs.

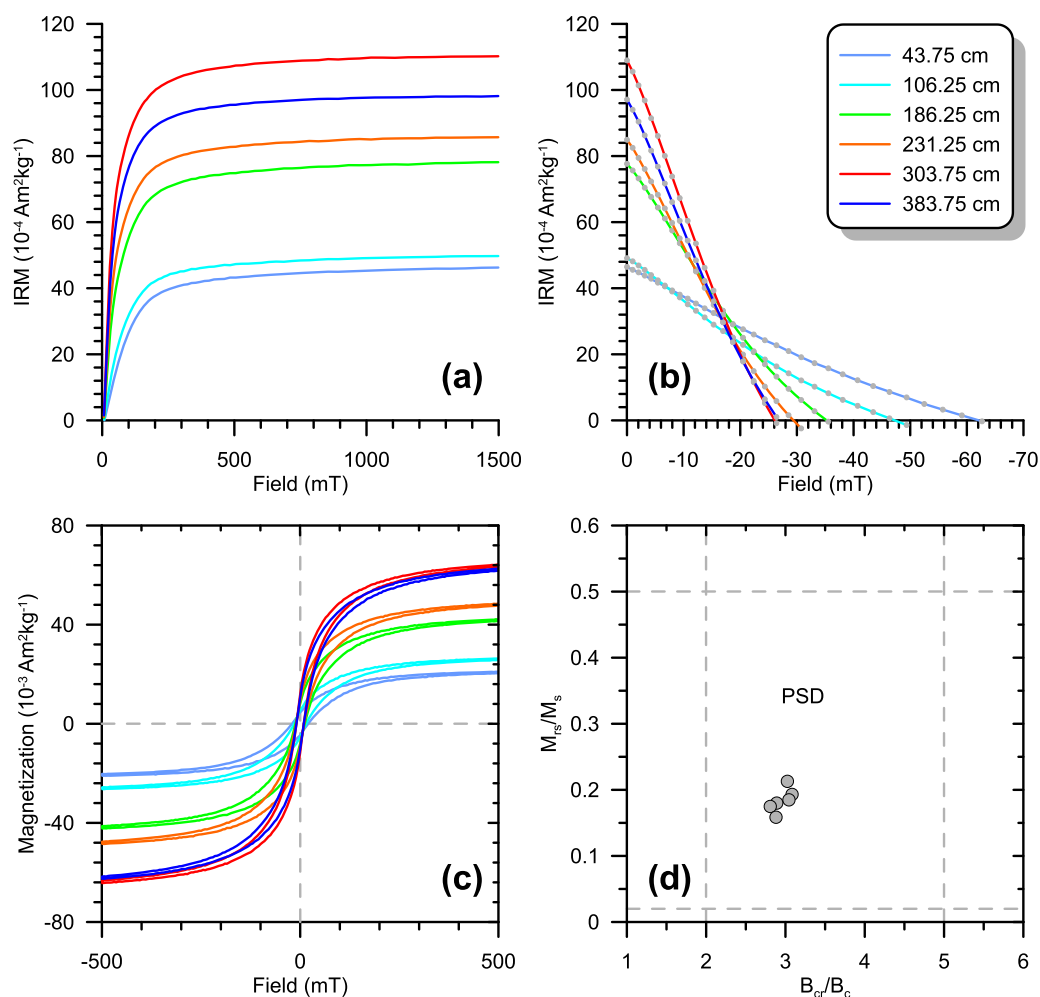


Figure 4. (a) Isothermal remanent magnetization (IRM) acquisition curves. (b) Backfield demagnetization of saturation IRM. (c) Hysteresis loops, after subtraction of the paramagnetic contribution. (d) Hysteresis ratios plotted on a Day plot [Day *et al.*, 1977; Dunlop, 2002]. PSD, pseudo-single domain. Depth of the measured samples are marked in the legend (b). Samples at 43.75 and 106.25 cm are from L8, and others from S8.

maghemite particles via pedogenesis [e.g., Zhou *et al.*, 1990; An *et al.*, 1991; Hao and Guo, 2005; Hao *et al.*, 2012]. By correlating χ curves of the XF, LC, and MS sections, six representative climatic tie points are selected, named as C1–C6 (Figure 7). Following the method used by De Menocal *et al.* [1990] and Liu *et al.* [2008], depth values of C1–C6 are plotted for every two sections (Figure 8). Theoretically, if there is no distinct pDRM offsets, the depth point of the MBB should be plotted on the correlation trend. In contrast, the locations of the MBB nearly all deviate from the correlation trend (Figure 8), which indicates the presence of potential offsets. We define the horizontal or vertical distance of the MBB from the stratigraphic trend as relative downward offset values for the pDRM between every two sections, but not the absolute offset depth for each single section. The relative offset of the upper and lower MBB varies from 3.14 to 42.09 cm, with exception of 72.80 cm derived from correlation between MS and XF sections, and varies from 2.33 to 37.84 cm for the middle MBB (Table 1). The mean of all the nine depth values is 30.9 cm. However, we should clarify that the pDRM offset in this study is a minimum estimation owing to only limited factors considered in this conceptual estimation.

4. Discussion

4.1. Factors Influencing the Downward Offset Depth of the pDRM

The NRM of Chinese loess mainly consist of VRM [Pan *et al.*, 2001], (p)DRM, and chemical remanent magnetization [Heller and Liu, 1984; Spassov *et al.*, 2003; Liu and Zhang, 2013]. The detrital magnetite particles (involving LC,

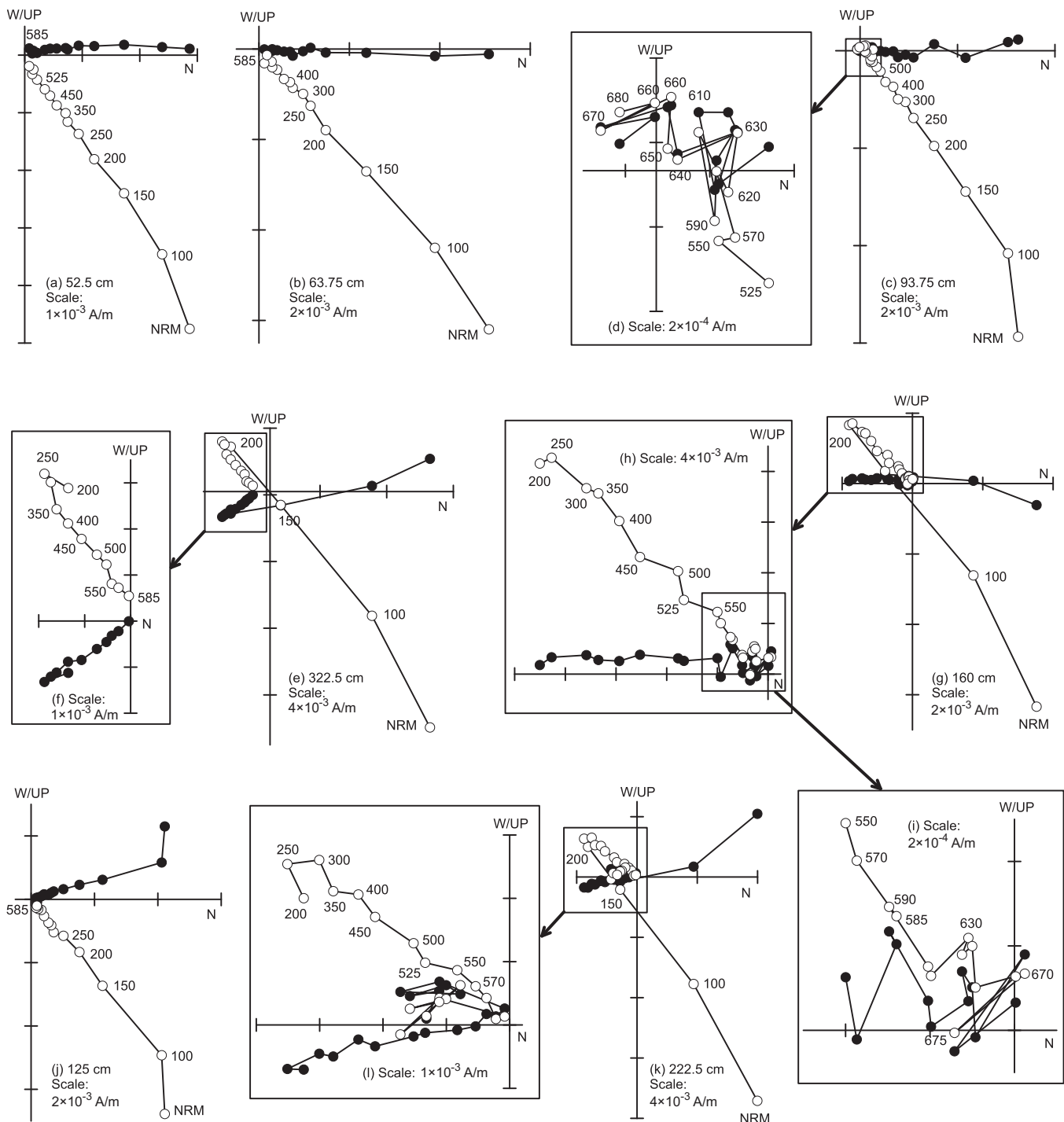


Figure 5. Orthogonal projections of progressive thermal demagnetization of natural remanent magnetization (NRM) for seven representative specimens at the Xifeng section. Solid (open) circles represent projections onto the horizontal (vertical) plane. Demagnetization temperature is given in degrees Celsius. Samples at (a, b) 52.5 and 63.75 cm are from L8, the Brunhes subchron. Samples at (c, g, j, k) 93.75, 160, 125, 222.5 cm belong to the MB transitional zone. Sample at (e) 322.5 cm is from S8, the Matuyama subchron.

MS, and XF in this study) carry a pDRM [Zhu *et al.*, 1994a, 1994b, 1999; Yang *et al.*, 2007a, 2008, 2010; Liu *et al.*, 2008], which is influenced by the postdepositional physical, chemical, and biological processes [Zhou and Shackleton, 1999]. Here we focused on effects of the sedimentation rate, precipitation, and degree of porosity.

Based on the optically stimulated luminescence chronology, the timing of the Laschamp excursion was estimated to be about 42–43 ka at Gulang section, significantly younger than that at Luochuan (about 47–51 ka)

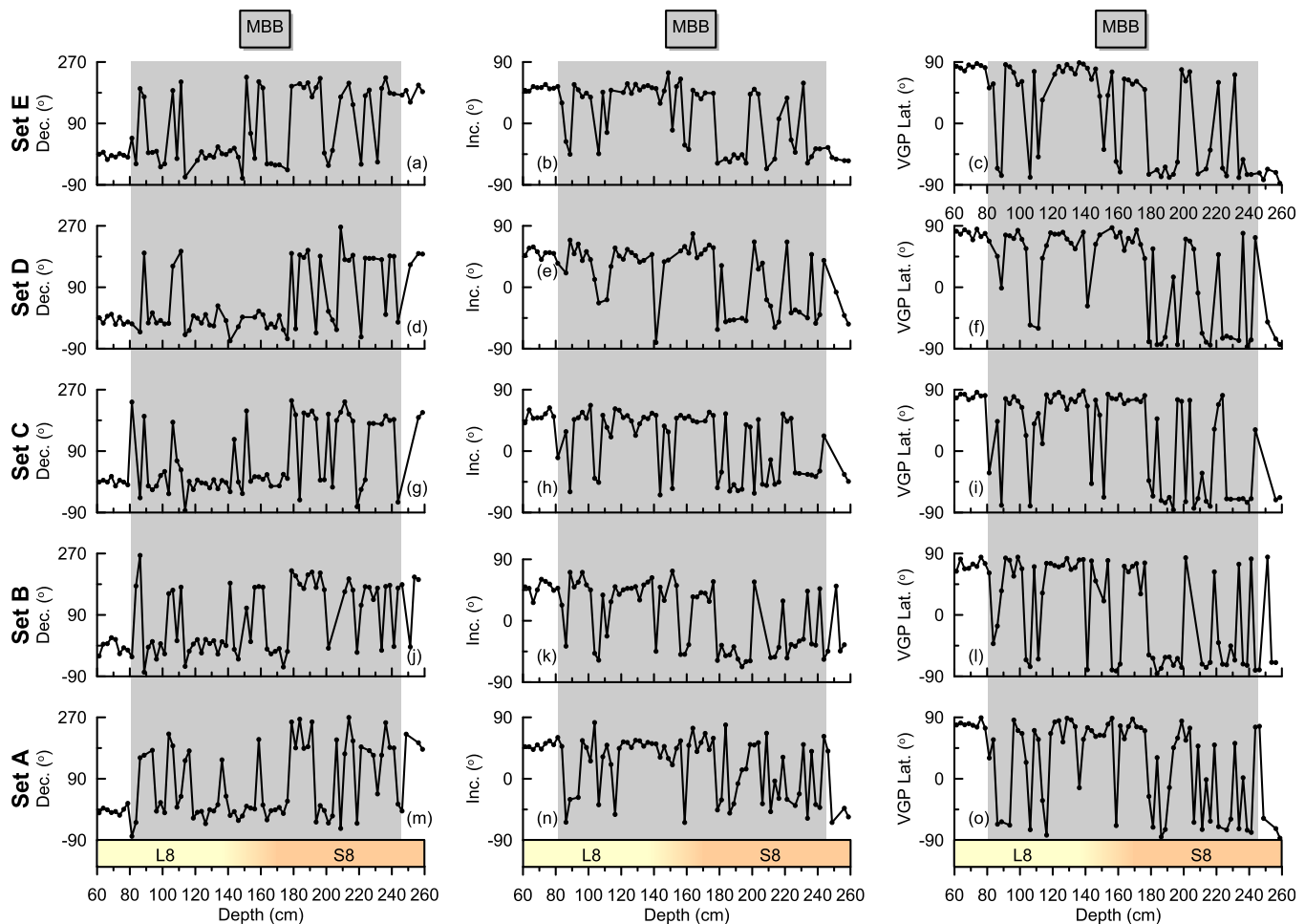


Figure 6. Magnetic stratigraphy of L8 and S8 in the 60–260 cm interval from the Xifeng section. Sets of A–E are parallel samples. Dec, Inc, VGP Lat are shown in the left, middle, and right columns, respectively. The MB transitional zone is shaded in gray.

and Weinan (about 54–57 ka) sections [Sun *et al.*, 2013]. Sun *et al.* [2013] revealed a trend of progressive south-eastward increase of the pDRM offset in the CLP, and they pointed that high sediment rates and low paleoprecipitation could result in a weaker offset effect. However, this model yielded from the late Pleistocene loess is inapplicable for the middle Pleistocene loess in MS areas which has both higher precipitation and sediment rate relative to LC and XF (Figures 8a and 8b).

Degree of loess porosity may be another factor that could influence the offset effect. Loess's interstitial void could release remanence carrying grains, and even result in realignment of these particles along ambient field [Løvlie *et al.*, 2011; Wang *et al.*, 2014]. Here we employ volume-weight as a proxy of porosity for loess sediments. Higher volume-weight value represents a lower porosity [Sun *et al.*, 1999]. Stratigraphic interval of the MBB in LC has higher volume-weight values than those in both MS and XF (Figure 9). Volume-weight values are almost consistent for the latter two sections during the MB reversal. Although lower degree of porosity in LC corresponds to relatively weaker offset effect (Figure 8b), the apparent difference in the pDRM downward offset between MS and XF cannot be well explained by porosity because these two profiles have similar porosity values (Figures 8a and 9).

Loess sedimentological redeposition experiments carried by Wang and Løvlie [2010] and Zhao and Roberts [2010] revealed that dry, unconsolidated redeposited sediments carry a magnetization with significantly shallower inclination compared to the ambient field. However, the moderate wetting redeposited sediments give rise to a better aligned magnetization because wetting of the dry and loose loess causes partial aggregation of grains (by increasing their cohesiveness). These experiments suggested that the capability

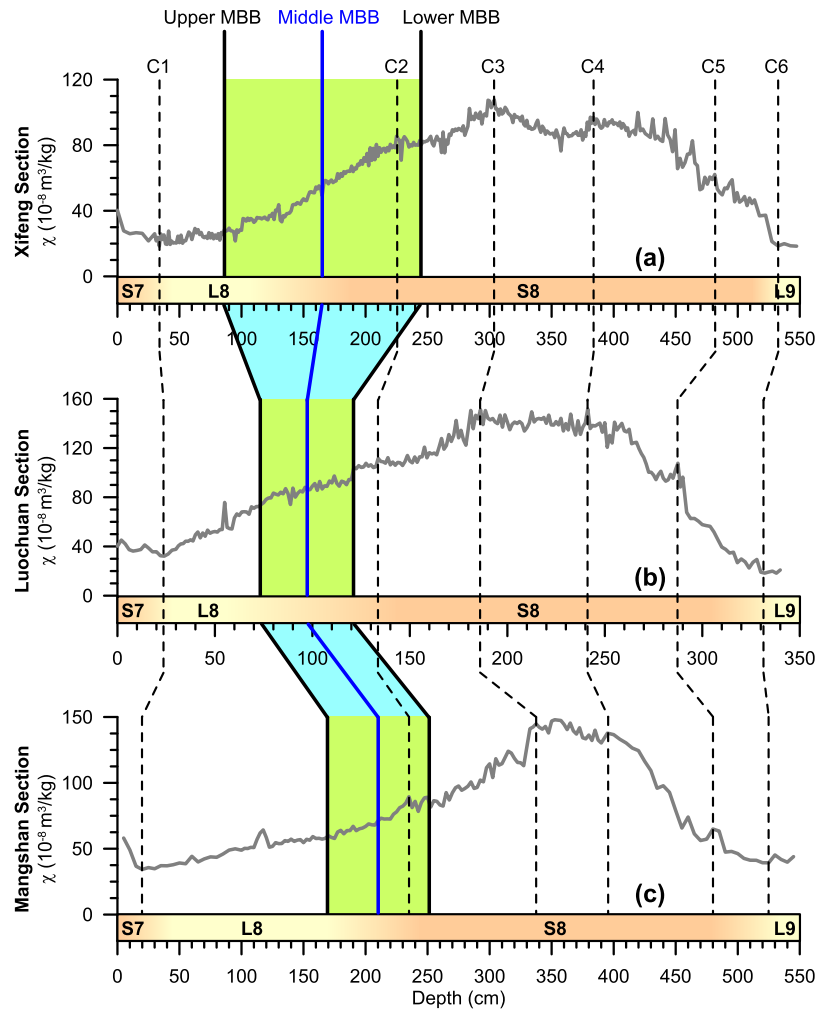


Figure 7. Susceptibility correlations of L8 and S8 from (a) Xifeng, (b) Luochuan [Jin and Liu, 2010], (c) Mangshan [Jin and Liu, 2011a] sections. Dashed lines C1–C6 are representative climatic points for the above sections, respectively. The MB transitional zones are shaded in green.

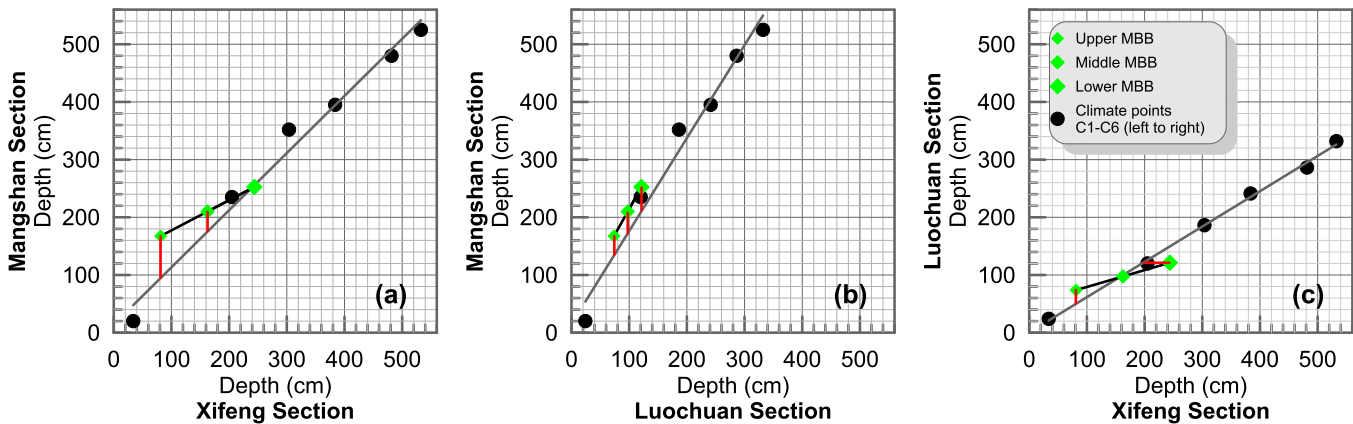


Figure 8. Depth plots of representative points between every two selected sections. Dots are representative climatic points (C1–C6). Diamonds are depth plots of the upper MBB, middle MBB, and the lower MBB, respectively. Gray lines are stratigraphic trend after linear fits from C1–C6. Short red lines mean the potential downward offset of the postdepositional remanent magnetization (pDRM).

Table 1. Relative pDRM Offset During the MB Reversal Among LC, XF, and MS Sections

| | Upper MBB (cm) | Middle MBB (cm) | Lower MBB (cm) |
|-------------------|----------------|-----------------|----------------|
| LC relative to XF | 23.64 | -2.33 | -28.31 |
| MS relative to XF | 72.80 | 34.83 | -3.14 |
| LC relative to MS | 33.59 | 37.84 | 42.09 |

of the deposited loess dust to acquire a pDRM is enhanced with moderate water content in sediments [Wang and Løvlie, 2010; Zhao and Roberts, 2010].

For natural loess, moderate paleoprecipitation will moisten the initially deposited loess dust, causing aggregation of loess particles that carry a better magnetization [Zhou et al., 2000]. Most

grains are locked in cohesive aggregates, while a small fraction of grains remain mobile [Wang and Løvlie, 2010]. This could be the pDRM acquisition mechanism for the northwestern CLP loess with limited and/or moderate precipitation, even for the hinterland CLP loess, such as LC and XF. During successive exposures to rain, wetting may allow mobile grains to realign thereby reducing the initial magnetization [Wang and Løvlie, 2010]. Rainfall-controlled leaching would enhance this process and lead to a larger pDRM offset [Løvlie et al., 2011; Wang et al., 2014]. While in the southeastern CLP loess, this leaching could be another mechanism for the pDRM lock-in. Although L8 of XF section is thinner than that of MS section, the MB transitional zone in XF is thicker than that in MS. This could be caused by relatively larger pDRM offset in MS, especially for the upper MBB (Figure 8a).

Based on above analysis, we propose that paleoprecipitation might be the dominant factor for the middle Pleistocene loess which influences the pDRM offset as Sun et al. [2013] suggested for loess since the last interglacial period.

4.2. Magnetization Mechanism of the MBB

In XF, the ChRMs of multiple subsets of parallel samples are inconsistent during the MB transition, whereas keeping agreement outside the transition (Figure 6). This behavior is consistent with paleomagnetic results of the MBB in LC [Jin and Liu, 2010] and MS [Jin and Liu, 2011a]. For Chinese loess, there is a SML before compaction of deposited dust [e.g., Sun et al., 2010]. It can simply shift the paleomagnetic record downward without necessarily filtering the signal [Liu et al., 2008]. In contrast, lock-in processes serve as a low-band pass filter. High-frequency features will be filtered out even for relatively shallow lock-in depths [Roberts and Winklhofer, 2004; Liu et al., 2008]. Therefore, with exception of lower intensity of geomagnetic field during the MB reversal which may reduce the alignment efficiency of the ChRM carriers along the ancient geomagnetic field, the inconsistencies of the ChRM directions records during the MB transition in XF (Figure 6), LC, and MS could also be caused by the potential pDRM lock-in effect.

The MBB paleomagnetic results of five sets of parallel samples in XF, MS, and LC are plotted in one graph (Figures 10b–10d), respectively. In Figure 11, we propose a conceptual model to explain the pDRM acquisition processes of Chinese loess during the MB transition. Here we define the location of the upper and lower MBB as D1, D2, D3, D4, and D4' during different status of the MB transition (D refers to an unknown depth value), respectively. Step I shows the initial status of loess sediments in the Matuyama subchron (Figure 11a). In Step II, paleomagnetic field began to reverse at the depth D3 (Figure 11b) and finished at the

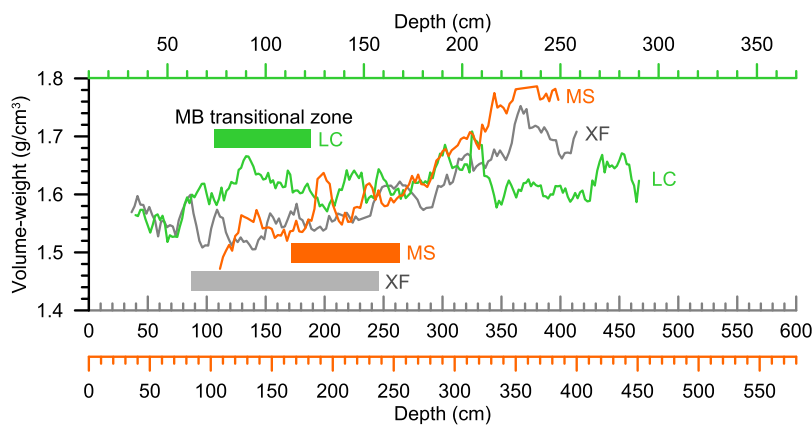


Figure 9. Volume-weight curves for part of L8 and S8 from Mangshan (orange), Xifeng (gray), and Luochuan (green) sections. Colorized horizon bars mean the MB transitional zones for the three sections, respectively.

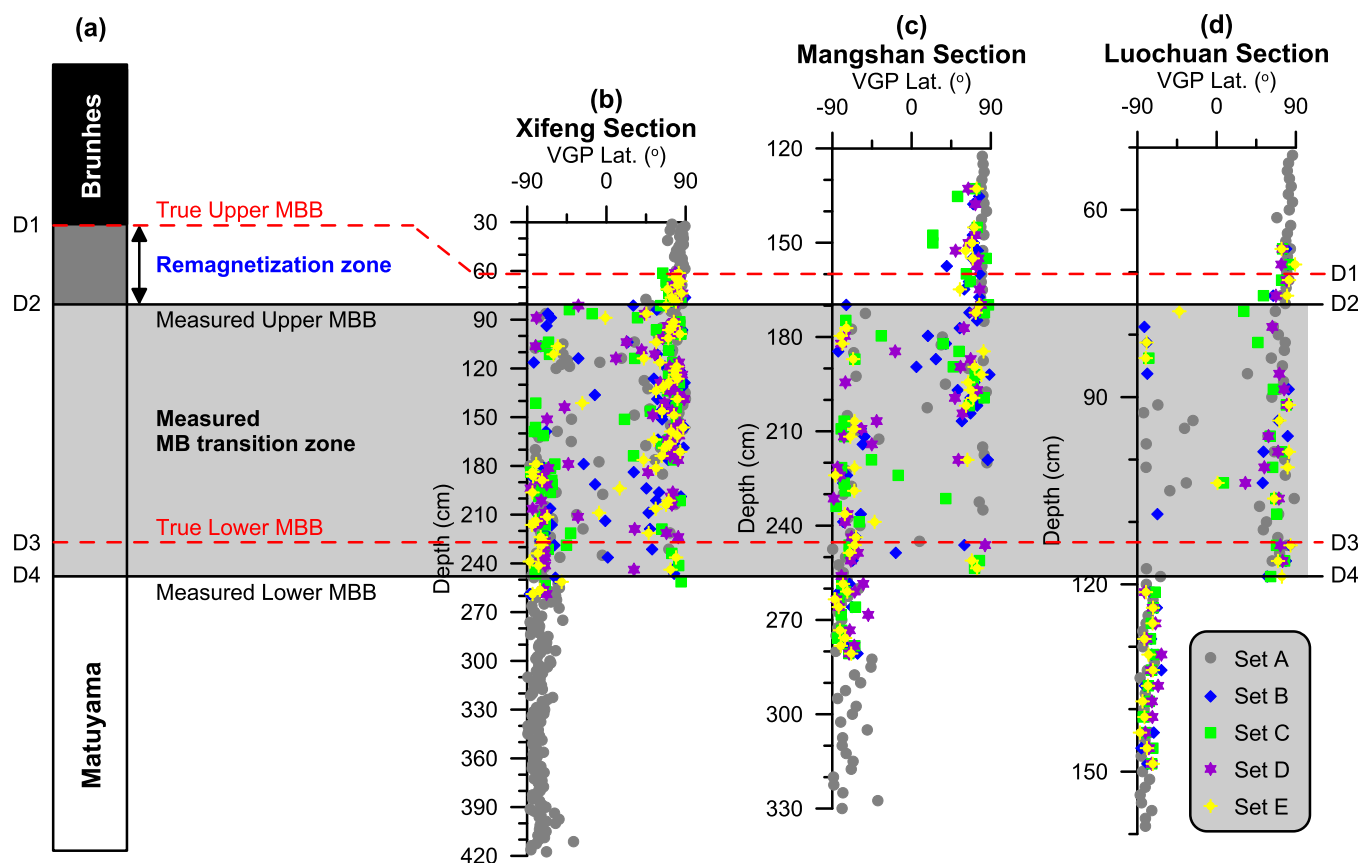


Figure 10. (a) Compiled VGP latitude of five sets of parallel samples of the Matuyama-Brunhes transition in (b) Xifeng, (c) Mangshan [Jin and Liu, 2011a], and (d) Luochuan [Jin and Liu, 2010] loess sections, respectively. D1 and D3 indicate the true MBB. D2 and D4 indicate the measured MBB.

depth D1 in Step III (Figure 11c). The lower MBB shifted downward at an intervening depth of D4' (not the final location). After an unknown period, the MBB was finally locked-in in Step IV (Figure 11d). Owing to potential lock-in effect (Figure 7), the measured upper MBB should be fixed downward from D1 to D2 (Figures 10a and 11d). However, the interval above the measured upper MBB between D1 and D2 has “abnormal” polarity (normal) (Figure 10). Therefore, we proposed that this interval with normal polarity should be a completely remagnetized zone by normal polarity overprint during the Brunhes subchron developed during processes of rainfall-controlled leaching (Figure 11d). This leaching could even decrease the fidelity of paleomagnetic record for the MB transition, even leading a remagnetization as proposed by Wang *et al.* [2014]. This behavior is also supported by in situ experiments which suggested that release and subsequent realignment of a fraction of the ChRM carriers could indeed yield a partial pDRM remagnetization [Løvlie *et al.*, 2011]. Recently, a new study from the Sulmona basin (central Italy) displayed that the MB transition occurred at about 786 ka ago [Sagnotti *et al.*, 2016]. This age is generally older than recently reported ages near 770 ka of the MBB [e.g., Channell *et al.*, 2010; Saganuma *et al.*, 2010, 2015]. In addition, no intermediate polarity was revealed during the MB transition. One possibility is that “the detailed MBB record is lost because it is overprinted” as Sagnotti *et al.* [2016] suggested. This behavior is consistent with our conceptual model that the stratigraphy interval above the MBB and upper part of the MBB is remagnetized.

Samples with normal polarity are more in the upper part of the MB transitional zone than in the lower MB zone in both XF and MS, vice versa (Figures 10b and 10c). This behavior indicates that the measured normal polarity in the MB transition zone should contain part of remagnetized polarity especially in the upper part of the MB transition zone owing to rainfall-controlled leaching (small moss green squares in Figure 11d between D2 and D3). Meanwhile, owing to downward offset of the lower MBB, the polarity in the lower part of the measured MB transition zone should be a mixture of geomagnetic information consisting of the residual Matuyama subchron (small chartreuse squares in Figure 11d between D3 and D4), true MB reversal, even part of remagnetized polarity (small moss green squares in Figure 11d between D3 and D4).

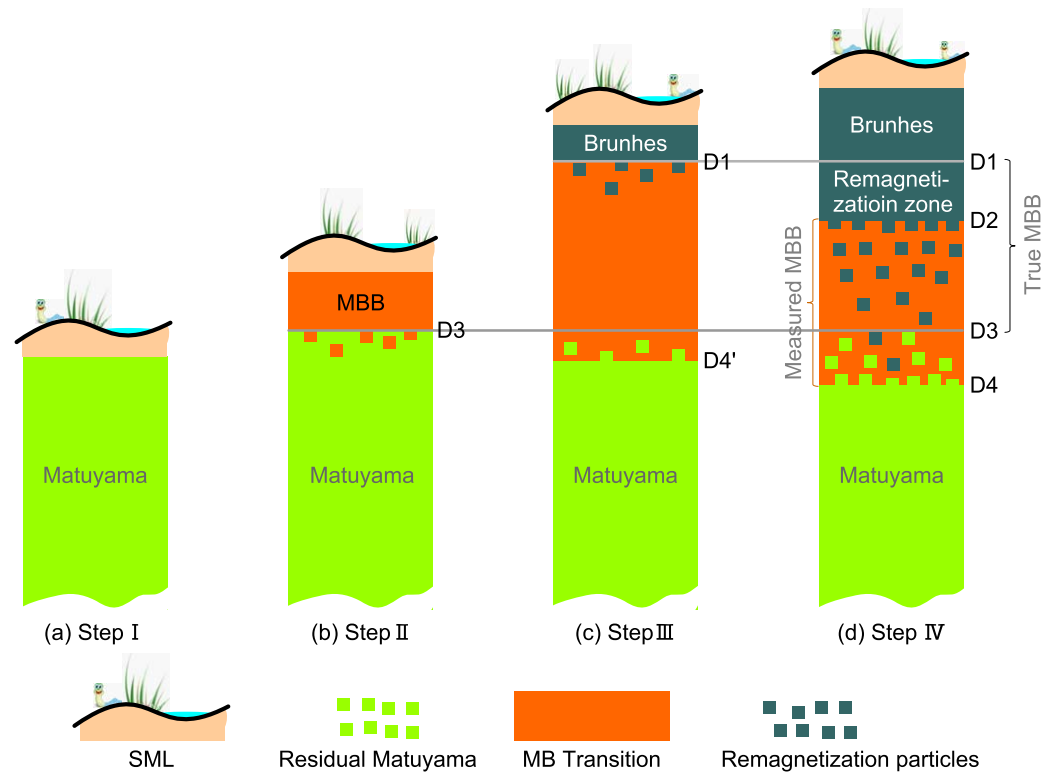


Figure 11. A conceptual model showing the postdepositional remanent magnetization mechanism of the Matuyama-Brunhes transition in Chinese loess. D1 and D3 indicate the true MBB. D2 and D4 indicate the measured MBB. SML, surface mixed layer.

Therefore, we further emphasize that the measured MB transitional zone in these three sections could not faithfully record true geomagnetic transition information owing to multiple factors, such as decreased alignment efficiency of the ChRM carriers, remagnetization (especially in the upper part of the measured polarity zone), residual polarity of the Matuyama in the lower part of the measured polarity transition zone. However, we should note that normal polarity samples dominant the lower measured MB transition zone in LC (Figure 10d) but not reverse polarity as XF and MS. This characteristic indicates a relatively weaker downward offset of the lower MBB, supported by depth plots of the bottom MBB (Figures 8b and 8c) where MS and XF display larger relatively downward offset.

Although different scale of lock-in effect exists in the CLP, a scale around several to tens of centimeters of downward offset for the MBB should not be larger enough to make us to locate the MBB in paleosol unit S7 as proposed by Zhou and Shackleton [1999]. Actually, downward offset of the NRM involves a SML and an underlying pDRM lock-in depth (containing a remagnetization zone). Thickness of the SML in Chinese loess has been estimated to be less than 20 cm in the western CLP, and about 5 cm in the central CLP [Sun *et al.*, 2010]. Deducting the SML effect, the pDRM lock-in depth during the MB reversal is proposed to be in a smaller scale. Therefore, the MBB in Chinese loess could be considered as a tie point after moderate upward adjustment, especially for previous loess magnetostratigraphy studies with relatively lower sampling resolution (generally larger than 20 cm interval). It is convincible to correlate L8/S8 to MIS 18/19 as recent studies suggested [Wang *et al.*, 2006; Liu *et al.*, 2008; Jin and Liu, 2011a, 2011b; Jin *et al.*, 2012]. Here we finally propose that loess-paleosol sequences in the central and/or the northwestern CLP are more suitable for astronomical timescales using orbital tuning relative to loess in the southeastern CLP with larger pDRM lock-in effect.

5. Conclusion

The MB transitional zone in the Xifeng loess section was newly determined with five sets of parallel specimens in a 162.5 cm interval. ChRM directions also show inconsistency during the MB reversal and show high consistency outside of the transitional zone as records in the Luochuan and Mangshan sections. This behavior could

be caused by combining the relative intensity and the potential pDRM lock-in effect driven by rainfall-controlled leaching during the reversal. The measured MB transition zone should be a mixture of geomagnetic information consisting of part of remagnetized polarity, reversal information, and the residual Matuyama subchron.

Depth plots of representative climatic and MBB points reveal several to tens of centimeters downward offset of the pDRM lock-in effect which is larger in the southeastern CLP relative to the central CLP. We propose that paleoprecipitation might be the dominant factor which influences the pDRM offset effect. Relatively larger scale of the pDRM offset in the southeastern CLP could be attributed to larger scale of rainfall-controlled leaching which could release some ChRM carriers, and moves them downward. While in the central CLP, moderate paleoprecipitation yields a weaker lock-in effect, even enhances the pDRM fixing, especially in the northwestern CLP with limited precipitation. Finally, the MBB in the central CLP could be considered as an isochronous chronological control after moderate upward adjustment. A convincing case can then be made to correlate L8/S8 to MIS 18/19.

Acknowledgments

This work was jointly funded by the National Basic Research Program of China (2013CB956403), the "Strategic Priority Research Program" of the CAS (XDB03020102), Chinese Continental Shelf Deep Drilling Program (GZH201100202), and the NSFC (41373073, 41025013, 41004023, and 41272202). Thanks to the three reviewers for their constructive comments and helpful suggestions on an earlier version of the manuscript. Supporting data are included in a Supporting Information pdf file; any additional data may be obtained from C.S. Jin (e-mail: csjin@mail.iggcas.ac.cn).

References

- An, Z. S., J. K. Geogre, S. C. Porter, and J. L. Xiao (1991), Magnetic susceptibility evidence of monsoon variation on the loess plateau of central China during the last 130,000 years, *Quat. Res.*, *36*, 29–36.
- Channell, J. E. T., D. A. Hodell, B. S. Singer, and C. Xuan (2010), Reconciling astrochronological and $^{40}\text{Ar}/^{39}\text{Ar}$ ages for the Matuyama-Brunhes boundary and late Matuyama Chron, *Geochem. Geophys. Geosyst.*, *11*, Q0AA12, doi:10.1029/2010GC003203.
- Day, R., M. Fuller, and V. A. Schmidt (1977), Hysteresis properties of titanomagnetite: Grain-size and compositional dependence, *Phys. Earth Planet. Inter.*, *13*, 260–266.
- De Menocal, P. B., W. F. Ruddiman, and D. V. Kent (1990), Depth of post-depositional remanence acquisition in deep-sea sediments: A case study of the Brunhes-Matuyama reversal and oxygen isotopic Stage 19.1, *Earth Planet. Sci. Lett.*, *99*, 1–13.
- Deng, C. L., R. X. Zhu, K. L. Verosub, M. J. Singer, and B. Y. Yuan (2000), Paleoclimatic significance of the temperature-dependent susceptibility of Holocene loess along a NW-SE transect in the Chinese loess plateau, *Geophys. Res. Lett.*, *27*(22), 3715–3718.
- Deng, C. L., N. J. Vidic, K. L. Verosub, M. J. Singer, Q. S. Liu, J. Shaw, and R. X. Zhu (2005), Mineral magnetic variation of the Jiaodao Chinese loess/paleosol sequence and its bearing on long-term climatic variability, *J. Geophys. Res.*, *110*, B03103, doi:10.1029/2004JB003451.
- Deng, C. L., J. Shaw, Q. S. Liu, Y. X. Pan, and R. X. Zhu (2006), Mineral magnetic variation of the Jingbian loess/paleosol sequence in the northern Loess Plateau of China: Implications for Quaternary development of Asian aridification and cooling, *Earth Planet. Sci. Lett.*, *241*(1–2), 248–259.
- Ding, Z. L., Z. W. Yu, N. W. Rutter, and T. S. Liu (1994), Towards an orbital time scale for Chinese loess deposits, *Quat. Sci. Rev.*, *13*, 39–70.
- Ding, Z. L., E. Derbyshire, S. L. Yang, Z. W. Yu, and S. F. Xiong (2002), Stacked 2.6-Ma grain size record from the Chinese loess based on five sections and correlation with the deep-sea $\delta^{18}\text{O}$ record, *Paleoceanography*, *17*(3), 1033, doi:10.1029/2001PA000725.
- Dunlop, D. J. (2002), Theory and application of the Day plot (M_r/M_s versus H_c/H_i): 1. Theoretical curves and tests using titanomagnetite data, *J. Geophys. Res.*, *107*(B3), 2056, doi:10.1029/2001JB000486.
- Hao, Q. Z., and Z. T. Guo (2005), Spatial variations of magnetic susceptibility of Chinese loess for the last 600 kyr: Implications for monsoon evolution, *J. Geophys. Res.*, *110*, B12101, doi:10.1029/2005JB003765.
- Hao, Q. Z., L. Wang, F. Oldfield, S. Z. Peng, L. Qin, Y. Song, B. Xu, Y. S. Qiao, J. Bloemendal, and Z. T. Guo (2012), Delayed build-up of Arctic ice sheets during 400,000-year minima in insolation variability, *Nature*, *490*, 393–396.
- Heller, F., and T. S. Liu (1982), Magnetostratigraphical dating of loess deposits in China, *Nature*, *300*, 431–433.
- Heller, F., and T. S. Liu (1984), Magnetism of Chinese loess deposits, *Geophys. J. R. Astron. Soc.*, *77*, 125–141.
- Heslop, D., C. G. Langereis, and M. J. Dekkers (2000), A new astronomical timescale for the loess deposits of Northern China, *Earth Planet. Sci. Lett.*, *184*, 125–139.
- Hunt, C. P., S. K. Banerjee, J. M. Han, P. A. Solheid, E. Oches, W. W. Sun, and T. Liu (1995), Rock-magnetic proxies of climate change in the loess-paleosol sequences of the western Loess Plateau of China, *Geophys. J. Int.*, *123*(1), 232–244.
- Jin, C. S., and Q. S. Liu (2010), Reliability of the natural remanent magnetization recorded in Chinese loess, *J. Geophys. Res.*, *115*, B04103, doi:10.1029/2009JB006703.
- Jin, C. S., and Q. S. Liu (2011a), Revisiting the stratigraphic position of the Matuyama-Brunhes geomagnetic polarity boundary in Chinese loess, *Palaeogeogr. Palaeoclimatol. Palaeoecol.*, *299*, 309–317.
- Jin, C. S., and Q. S. Liu (2011b), Remagnetization mechanism and a new age model for L9 in Chinese loess, *Phys. Earth Planet. Inter.*, *187*, 261–275.
- Jin, C. S., Q. S. Liu, and J. C. Larrasoana (2012), A precursor to the Matuyama-Brunhes reversal in Chinese loess and its palaeomagnetic and stratigraphic significance, *Geophys. J. Int.*, *190*, 829–842.
- Kirschvink, J. L. (1980), The least-squares line and plane and the analysis of palaeomagnetic data, *Geophys. J. R. Astron. Soc.*, *62*, 699–718.
- Løvlie, R., R. H. Wang, and X. S. Wang (2011), In situ remagnetization experiments of loess on the Chinese Loess Plateau: Evidence for localized post-depositional remanent magnetization, *Geochem. Geophys. Geosyst.*, *12*, Q12015, doi:10.1029/2011GC003830.
- Liu, Q. S., S. K. Banerjee, and M. J. Jackson (2003), An integrated study of the grain-size-dependent magnetic mineralogy of the Chinese loess/paleosol and its environmental significance, *J. Geophys. Res.*, *108*(B9), 2437, doi:10.1029/2002JB002264.
- Liu, Q. S., C. L. Deng, Y. Yu, J. Yorrent, M. J. Jackson, S. K. Banerjee, and R. X. Zhu (2005), Temperature dependence of magnetic susceptibility in an argon environment: Implications for pedogenesis of Chinese loess/paleosols, *Geophys. J. Int.*, *161*, 102–112.
- Liu, Q. S., A. P. Roberts, E. J. Rohling, R. X. Zhu, and Y. B. Sun (2008), Post-depositional remanent magnetization lock-in and the location of the Matuyama-Brunhes geomagnetic reversal boundary in marine and Chinese loess sequences, *Earth Planet. Sci. Lett.*, *275*, 102–110.
- Liu, Q. S., C. S. Jin, P. X. Hu, Z. X. Jiang, K. P. Ge, and A. P. Roberts (2015), Magnetostratigraphy of Chinese loess-paleosol sequences, *Earth Sci. Rev.*, *150*, 139–167.
- Liu, W. M., and L. Y. Zhang (2013), Chemical magnetization in Chinese loess, *Phys. Earth Planet. Inter.*, *218*, 14–18.
- Lu, H. Y., X. D. Liu, F. Q. Zhang, Z. S. An, and D. John (1999), Astronomical calibration of loess-paleosol deposits at Luochuan, central Chinese Loess Plateau, *Palaeogeogr. Palaeoclimatol. Palaeoecol.*, *154*(3), 237–246.

- Pan, Y. X., R. X. Zhu, J. Shaw, Q. S. Liu, and B. Guo (2001), Can relative paleointensities be determined from the normalized magnetization of the wind-blown loess of China?, *J. Geophys. Res.*, *106*(B9), 19,221–19,232.
- Pan, Y. X., R. X. Zhu, Q. S. Liu, B. Guo, L. P. Yue, and H. N. Wu (2002), Geomagnetic episodes of the last 1.2 Myr recorded in Chinese loess, *Geophys. Res. Lett.*, *29*(8), 123-1–123-14.
- Porter, S. C., and Z. S. An (1995), Correlation between climate events in the North Atlantic and China during the last glaciation, *Nature*, *375*, 305–308.
- Roberts, A. P., and M. Winklhofer (2004), Why are geomagnetic excursions not always recorded in sediments? Constraints from post-depositional remanent magnetization lock-in modelling, *Earth Planet. Sci. Lett.*, *227*(3–4), 345–359.
- Roberts, A. P., Y. L. Cui, and K. L. Verosub (1995), Wasp-waisted hysteresis loops: Mineral magnetic characteristics and discrimination of components in mixed magnetic systems, *J. Geophys. Res.*, *100*(B9), 17,909–17,924.
- Sagnotti, L., B. Giaccio, J. C. Liddicoat, S. Nomade, P. R. Renne, G. Scardia, and C. J. Sprain (2016), How fast was the Matuyama-Brunhes geomagnetic reversal? A new subcentennial record from the Sulmona Basin, central Italy, *Geophys. J. Int.*, *204*, 798–812.
- Spassov, S., F. Heller, M. E. Evans, L. P. Yue, and Z. L. Ding (2001), The Matuyama/Brunhes geomagnetic polarity transition at Lingtai and Baoji, Chinese Loess Plateau, *Phys. Chem. Earth. A*, *26*(11–12), 899–904.
- Spassov, S., F. Heller, M. E. Evans, L. P. Yue, and T. V. Dobeneck (2003), A lock-in model for the complex Matuyama-Brunhes boundary record of the loess/palaeosol sequence at Lingtai (Central Chinese Loess Plateau), *Geophys. J. Int.*, *155*, 350–366.
- Suganuma, Y., Y. Yokoyama, T. Yamazaki, K. Kawamura, C.-S. Horn, and H. Matsuzaki (2010), ¹⁰Be evidence for delayed acquisition of remanent magnetization in marine sediments: Implication for a new age for the Matuyama-Brunhes boundary, *Earth Planet. Sci. Lett.*, *296*, 443–450.
- Suganuma, Y., et al. (2015), Age of Matuyama-Brunhes boundary constrained by U-Pb zircon dating of a widespread tephra, *Geology*, *43*(6), 491–494.
- Sun, Y. B., J. Zhou, and Z. S. An (1999), The paleoclimate significance recorded by the compact-corrected climate proxy of late Tertiary eolian sequence on the Chinese Loess Plateau [in Chinese with English abstract], *Mar. Geol. Quat. Geol.*, *19*(4), 51–58.
- Sun, Y. B., S. C. Clemens, Z. S. An, and Z. W. Yu (2006), Astronomical timescale and palaeoclimatic implication of stacked 3.6-Myr monsoon records from the Chinese Loess Plateau, *Quat. Sci. Rev.*, *25*, 33–48.
- Sun, Y. B., X. L. Wang, Q. S. Liu, and S. C. Clemens (2010), Impacts of post-depositional processes on rapid monsoon signals recorded by the last glacial loess deposits of northern China, *Earth Planet. Sci. Lett.*, *289*, 171–179.
- Sun, Y. B., S. C. Clemens, C. Morrill, X. P. Lin, X. L. Wang, and Z. S. An (2011), Influence of Atlantic meridional overturning circulation on the East Asian winter monsoon, *Nat. Geosci.*, *5*, 46–49.
- Sun, Y. B., X. K. Qiang, Q. S. Liu, J. Bloemendal, and X. L. Wang (2013), Timing and lock-in effect of the Laschamp geomagnetic excursion in Chinese Loess, *Geochem. Geophys. Geosyst.*, *14*, 4952–4961, doi:10.1002/2013GC004828.
- Tauxe, L., T. Herbert, N. J. Shackleton, and Y. S. Kok (1996), Astronomical calibration of the Matuyama-Brunhes boundary: Consequences for magnetic remanence acquisition in marine carbonates and the Asian loess sequences, *Earth Planet. Sci. Lett.*, *140*, 133–146.
- Wang, R. H., and R. Løvlie (2010), Subaerial and subaqueous deposition of loess: Experimental assessment of detrital remanent magnetization in Chinese loess, *Earth Planet. Sci. Lett.*, *298*, 394–404.
- Wang, X. S., R. Løvlie, Z. Y. Yang, J. L. Pei, Z. Z. Zhao, and Z. M. Sun (2005), Remagnetization of Quaternary eolian deposits: A case study from SE Chinese Loess Plateau, *Geochem. Geophys. Geosyst.*, *6*, Q06H18, doi:10.1029/2004GC000901.
- Wang, X. S., Z. Y. Yang, R. Løvlie, Z. M. Sun, and J. L. Pei (2006), A magnetostratigraphic reassessment of correlation between Chinese loess and marine oxygen isotope records over the last 1.1 Ma, *Phys. Earth Planet. Inter.*, *159*, 109–117.
- Wang, X. S., R. Løvlie, Y. Chen, Z. Y. Yang, J. L. Pei, and L. Tang (2014), The Matuyama-Brunhes polarity reversal in four Chinese loess records: High-fidelity recording of geomagnetic field behavior or a less than reliable chronostratigraphic marker?, *Quat. Sci. Rev.*, *101*, 61–76.
- Yang, S. L., and Z. L. Ding (2010), Drastic climatic shift at ~2.8 Ma as recorded in eolian deposits of China and its implications for redefining the Pliocene-Pleistocene boundary, *Quat. Int.*, *219*, 37–44.
- Yang, T. S., M. Hyodo, Z. Y. Yang, and J. L. Fu (2007a), Two geomagnetic excursions during the Brunhes chron recorded in Chinese loess-palaeosol sediments, *Geophys. J. Int.*, *171*, 104–114.
- Yang, T. S., H. D. Li, J. L. Fu, M. Toshiaki, Z. Y. Yang, and H. Masayuki (2007b), Investigation on the lock-in depth of paleosol L₇ and loess L₈ in Baoji [in Chinese with English abstract], *Quat. Sci.*, *27*(6), 972–982.
- Yang, T. S., M. Hyodo, Z. Y. Yang, L. Ding, H. D. Li, J. L. Fu, S. B. Wang, H. W. Wang, and T. Mishima (2008), Latest Olduvai short-lived reversal episodes recorded in Chinese loess, *J. Geophys. Res.*, *113*, B05103, doi:10.1029/2007JB005264.
- Yang, T. S., M. Hyodo, Z. Y. Yang, H. D. Li, and M. Maeda (2010), Multiple rapid polarity swings during the Matuyama-Brunhes (M-B) transition from two high-resolution loess-paleosol records, *J. Geophys. Res.*, *115*, B05101, doi:10.1029/2009JB006301.
- Zhao, H., X. K. Qiang, and Y. B. Sun (2014), Apparent timing and duration of the Matuyama-Brunhes geomagnetic reversal in Chinese loess, *Geochem. Geophys. Geosyst.*, *15*, 4468–4480, doi:10.1002/2014GC005497.
- Zhao, X., and A. P. Roberts (2010), How does Chinese loess become magnetized?, *Earth Planet. Sci. Lett.*, *292*(1–2), 112–122.
- Zhou, L. P., and N. J. Shackleton (1999), Misleading positions of geomagnetic reversal boundaries in Eurasian loess and implications for correlation between continental and marine sedimentary sequences, *Earth Planet. Sci. Lett.*, *168*, 117–130.
- Zhou, L. P., F. Oldfield, A. G. Wintle, S. G. Robinson, and J. T. Wang (1990), Partly pedogenic origin of magnetic variations in Chinese loess, *Nature*, *346*(6286), 737–739.
- Zhou, L. P., N. J. Shackleton, and A. E. Dodonov (2000), Stratigraphical interpretation of geomagnetic polarity boundaries in Eurasian loess [in Chinese with an English abstract], *Quat. Sci.*, *20*(2), 196–202.
- Zhou, W. J., J. W. Beck, X. H. Kong, Z. S. An, X. K. Qiang, Z. K. Wu, F. Xian, and H. Ao (2014), Timing of the Brunhes-Matuyama magnetic polarity reversal in Chinese loess using ¹⁰Be, *Geology*, *42*(6), 467–470.
- Zhu, R. X., C. Laj, and A. Mazaud (1994a), The Matuyama-Brunhes and Upper Jaramillo transitions recorded in a loess section at Weinan, north-central China, *Earth Planet. Sci. Lett.*, *125*(1–4), 143–158.
- Zhu, R. X., L. P. Zhou, C. Laj, A. Mazaud, and Z. L. Ding (1994b), The Blake geomagnetic polarity episode recorded in Chinese loess, *Geophys. Res. Lett.*, *21*(8), 697–700.
- Zhu, R. X., Y. X. Pan, B. Guo, and Q. S. Liu (1998), A recording phase lag between ocean and continent climate changes: Constrained by the Matuyama/Brunhes polarity boundary, *Chin. Sci. Bull.*, *43*(19), 1593–1598.
- Zhu, R. X., Y. X. Pan, and Q. S. Liu (1999), Geomagnetic excursions recorded in Chinese loess in the last 70,000 years, *Geophys. Res. Lett.*, *26*(4), 505–508.
- Zhu, R. X., Q. S. Liu, and M. J. Jackson (2004), Paleoenvironmental significance of the magnetic fabrics in Chinese loess-paleosols since the last interglacial (<130 ka), *Earth Planet. Sci. Lett.*, *221*(1–4), 55–69.
- Zhu, R. X., Q. S. Liu, Y. X. Pan, C. L. Deng, R. Zhang, and X. F. Wang (2006), No apparent lock-in depth of the Laschamp geomagnetic excursion: Evidence from the Malan loess, *Sci. China (Earth Sci.)*, *49*(9), 960–967.